

# A simplified method to estimate kinetic and thermodynamic parameters on the solid–liquid separation of pollutants

G. Montes-Hernandez<sup>a,\*</sup>, S. Rihs<sup>b</sup>

<sup>a</sup> UMR 7566 UHP-CNRS, 54506 Vandoeuvre les-Nancy-Cedex, France

<sup>b</sup> UMR 7517 ULP-CNRS, CGS, 1 rue Blessig, F-67084 Strasbourg, France

Received 2 November 2005; accepted 31 January 2006

Available online 23 March 2006

## Abstract

The aim of the present study was to propose a simplified experimental–theoretical method for estimating the kinetic and thermodynamic parameters for the solid–liquid separation of pollutants by using kinetic studies with batch reactors, i.e., the removed quantity of dissolved ion as a function of time at different initial concentration. This method was applied to the removal of uranyl ion ( $\text{UO}_2^{2+}$ ) from aqueous solutions onto synthetic manganese oxide (birnessite). The pseudo-second-order kinetics and one-site saturation models were proposed to fit the experimental and calculated data, the fitting parameters being estimated by nonlinear regression, using the least-squares method. For initial concentration range 0.2–11.8  $\mu\text{M}$ , the results showed that the uranyl removal process in dispersed batch reactors can be efficiently modeled by the proposed models. Then, several kinetic and thermodynamic parameters were calculated, such as maximal removed quantity of uranyl,  $q_{r,\text{max}}$ , half-removal time,  $t_{1/2}$ , initial rate of uranyl-ion removal,  $v_0$ , initial uranyl-removal coefficient,  $K$ , maximal rate of uranyl removal,  $v_{0,\text{max}}$ , mass transfer coefficient,  $D_{\text{transfer}}$ , equilibrium Langmuir constant,  $K_L$ , and constant separation factor,  $K_s$ . These parameters make it possible to demonstrate that the removal of U onto birnessite is favorable, and that the maximum surface coverage of the uranyl ions represents about 3% of vacant sites in the Mn layer.

© 2006 Elsevier Inc. All rights reserved.

**Keywords:** Removal; Uranyl ions; Manganese oxide; Pseudo-second-order kinetics; One-site saturation models; Batch reactors

## 1. Introduction

### 1.1. General concepts

Adsorption at solid–liquid interfaces is important in technological processes and products such as corrosion, catalysis, nanoparticle ultracapacitors, molecular sieves, and semiconductor manufacturing [1]. In addition, the adsorption of surfactants at the solid–liquid interfaces is an important topic in numerous processes ranging from mineral beneficiation to detergency, including such applications as wastewater treatment and soil remediation, dispersion stabilization in ceramics and enhanced oil recovery [2,3].

In the literature numerous experimental studies on the solid–liquid separation of pollutants (ions and organic molecules) have been reported. These studies have been preferentially performed in the laboratory with batch reactors because of their easy operation and lower cost compared with column reactors. Unfortunately, numerous authors still report their experimental results in raw form (i.e., without fitting of data) or they systematically apply the classical models (e.g., Langmuir, Freundlich, Redlich–Peterson, and Brunauer–Emmett–Teller) in order to fit their experimental data. But they frequently neglect the importance of kinetic data. For this reason, the major objective of this study was to propose a simplified experimental–theoretical method for estimating the kinetic and thermodynamic parameters of solid–liquid separation of pollutants by using kinetic studies with batch reactors, i.e., the removed quantity of dissolved ions as a function of time at different initial concentrations. This method was applied to the removal of uranyl ions ( $\text{UO}_2^{2+}$ ) from aqueous solutions onto synthetic manganese ox-

\* Corresponding author.

E-mail address: [german.montes@g2r.uhp-nancy.fr](mailto:german.montes@g2r.uhp-nancy.fr)  
(G. Montes-Hernandez).

ide (hexagonal birnessite). Pseudo-second-order kinetics and one-site saturation models are proposed to fit the experimental and calculated data at low dissolved  $U^{VI}$  concentration. For this case, the fitting parameters can be estimated by nonlinear regression, using the least-squares method.

### 1.2. General description of manganese oxides

Birnessite and its related hydrated form buserite are the most common layered Mn oxides in natural environments [4]. Because of their microcrystallinity (resulting in high specific surface area), surface charge, high cation-exchange capacity, and redox properties, these minerals are known to have unusually high scavenging capacities for heavy metals (e.g., Co, Zn, Pb [5–8]). The affinity of radionuclides (U, Th, Ra, Pu) for Mn oxides has also been widely reported at every stage of radionuclide transport on earth [9–13]. The presence of an extremely small amount of Mn oxides (as low as 0.5%, for instance [12]) might be adequate to control the distribution of heavy metals and radionuclides between soil or sediment and aqueous systems. Yet most studies on the interactions between these minerals and radionuclides occurring in natural systems remain global, and very few detailed works have been realized.

The crystalline structure of buserite and its conversion to birnessite have been extensively studied [6,14–21]. These studies have established that Na-rich buserite (at high pH) consists of successive layers of Mn octahedra with a periodicity of 10 Å along the  $c$  axis and exchangeable cations and two layers of  $H_2O$  in its interlayer space. Partial dehydration of monoclinic buserite leads to the formation of a 7-Å layer spacing triclinic birnessite with various interlayer cations. Moreover, buserite also converts to a 7-Å layer spacing hexagonal birnessite  $[Mn_{0.05}^{2+}Mn_{0.12}^{3+}(Mn_{0.74}^{4+}Mn_{0.10}^{3+}\square_{0.17})O_{1.7}(OH)_{0.3}]$  [19] in acidic medium. This conversion results in the formation of vacant layer sites and the loss of exchangeable cations in the interlayer space. The layer charge is thus compensated for by interlayer protons and  $Mn^{3+}$  and  $Mn^{2+}$  cations (Fig. 1). Because the conversion of monoclinic to hexagonal birnessite is occurring at pH around 7, both types can be present in natural soils, each having different reactive surface properties. Distinction between these two forms in natural samples using conventional analytical techniques is usually difficult because of the defective, poorly crystallized structure of Mn soil minerals. However, some recent studies using powerful X-ray techniques succeeded in demonstrating that hexagonal birnessite is the one involved in the sequestration of several heavy metals in soils [17,22,23].

## 2. Materials and methods

Synthetic Na-rich buserite ( $Na_{0.3}Mn^{III,IV}O_2$ ) was prepared by oxidation process at high pH following the protocol described by Giovanoli et al. [24]. Immediately after the end of the oxidation, the crystals were kept in solution and aged at 120 °C for 48 h, yielding highly ordering crystals. The aged product was centrifuged and the supernatant discarded. The solid was then washed by centrifugation and redispersion in deionized

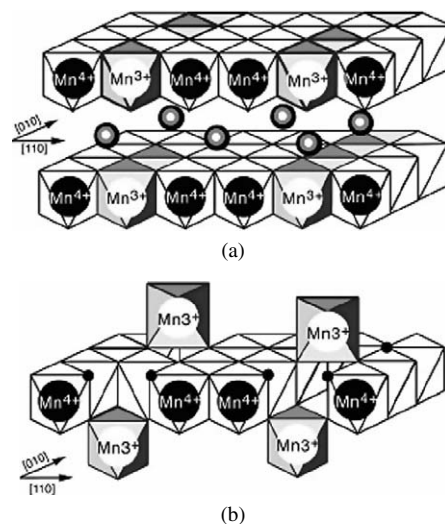


Fig. 1. Structure of triclinic birnessite (a) with Na interlayer cations and hexagonal (low pH) birnessite (b). After Drits et al. [17], Silvester et al. [18], and Lanson et al. [19].

water about 15 times. The resulting material was stored in suspension at 4 °C. Powder X-ray diffraction on solid (oven-dried at 60 °C) confirms the purity of the synthesized Na buserite and shows the diagnostic peaks (202 and 203 reflections at 2.03 and 1.71 Å, respectively) of hexagonal birnessite after equilibration to low pH [8,17,19]. A specific surface area of 11 m<sup>2</sup>/g was measured by the BET N<sub>2</sub> method.

Preparation of hexagonal birnessite by equilibration of Na-buserite to low pH was performed following a protocol similar to that of Silvester et al. [18]. In a batch reactor the appropriate amount of buserite suspension (corresponding to 1 g of solid) was suspended in 300 ml of ionic medium of 0.1 M NaClO<sub>4</sub> (previously boiled and bubbled with Ar gas). The suspension was continuously maintained under Ar to exclude CO<sub>2</sub> and stirred at a constant rate of 200 rpm. The initial pH of this suspension was equal to ~9.5. The suspension was equilibrated to pH 4 with an automatic titrator, by addition of HCl 0.1 M (about 30 ml of 0.1 M acid was necessary to reach equilibrium, achieved within less than 12 h). This pH was chosen to be in the range of hexagonal birnessite stability (<7) and above the pH of zero point of charge  $pH_{zpc}$  of the mineral (expected to be in the same range as  $\delta$ -MnO<sub>2</sub>, i.e., 2–3 [25], considering the analogy between both minerals). An appropriate amount of  $U^{VI}$  (in acidic solution) was then added to the suspension, the pH being readjusted to 4 by adding an appropriate amount of NaOH. The amount of added  $U^{VI}$  was precisely weighted to get initial concentrations ranging from 0.2 to 11.8  $\mu$ M. The evolution of the dissolved  $U^{VI}$  concentration was monitored by sampling the solution at various times. The experiments were performed at room temperature. A few cm<sup>3</sup> of the suspension were withdrawn and filtered through a 0.45- $\mu$ m Teflon filter. Adsorption on the filter and the filter holder was determined to be negligible. The filtered solution was immediately acidified and further diluted for measurement of  $U^{VI}$  by inductively coupled plasma mass spectrometry (Fisons VG-Plasma Quad ICP-MS). The experiments were maintained for several days but equilibrium was achieved within 20 h.

### 3. Results and discussion

#### 3.1. The removed quantity of uranyl ion ( $UO_2^{2+}$ )

Calculation of aqueous U speciation was performed using the MINTEQA2 3.11 code [26]. Thermodynamic data for aqueous uranyl species and solubility constants of U-bearing solid phases were adjusted to be consistent with the NEA database [27]. The formation constant of  $UO_2(OH)_2$  [28] and solubility constant of “amorphous” schoepite from Torrero et al. [29] were also added to the database. Calculation of U speciation shows that more than 96% of the  $U^{VI}$  occur as uranyl ions ( $UO_2^{2+}$ ) in the experimental suspensions over the entire range of U concentration. All the U-bearing solid phases in the database of MINTEQA2, were undersaturated in these solutions.

The removed quantity of uranyl ions on the dispersed particles of manganese oxide as a function of time can be calculated using the formula

$$q_{r,t} = \frac{C_0 - C_t}{m} V, \quad (1)$$

where  $C_0$  represents the initial concentration of uranyl ion [ $\mu\text{mol/L}$ ],  $C_t$  represents the concentration of uranyl ion at instant time  $t$  [ $\mu\text{mol/L}$ ],  $V$  represents the volume of the aqueous solution [L], and  $m$  represents the mass of synthetic manganese oxide [g].

The experimental kinetic curves concerning the removal of uranyl ion from aqueous solution onto synthetic manganese oxide are shown in Fig. 2. These curves show clearly that the removed quantity of uranyl ion increases with an increase in the initial concentration due to a high physicochemical affinity between solid particles of manganese oxide and uranyl ions.

#### 3.2. Fitting of kinetic curves

Several kinetic models including first-order, pseudo-first-order, second-order, pseudo-second-order, parabolic diffusion,

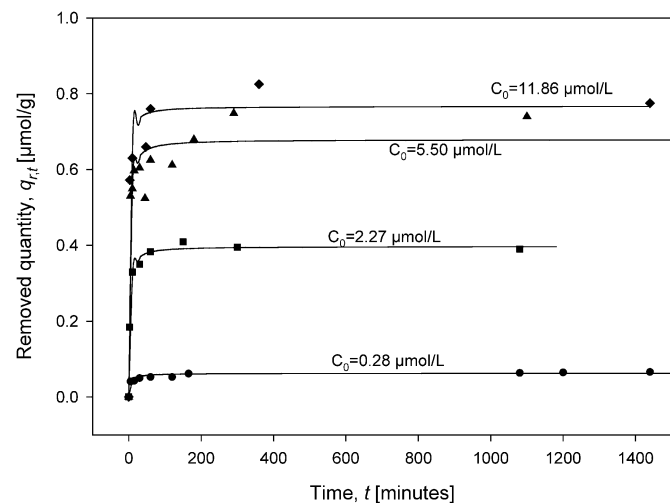


Fig. 2. Experimental kinetic curves for removal of the uranyl ion from aqueous solution onto synthetic manganese oxide.

and power function kinetic expressions are reported in the literature in order to fit the kinetic experimental data of a solid–liquid separation process. For our study, the best fit (attested by a correlation factor close to 1) of the experimental data was achieved using a pseudo-second-order kinetic model,

$$\frac{dq_{r,t}}{dt} = k_r(q_{r,\max} - q_{r,t})^2, \quad (2)$$

where  $k_r$  is the rate constant of removal for uranyl ions [ $\text{g}/\mu\text{mol min}$ ] for a given uranyl concentration,  $q_{r,\max}$  is the maximal removed quantity of uranyl or removed quantity of uranyl at equilibrium [ $\mu\text{mol/g}$ ], and  $q_{r,t}$  is the removed quantity of uranyl at any time  $t$  [ $\mu\text{mol/g}$ ].

The integrated form of Eq. (2) for the boundary conditions  $t = 0$  to  $t = t$  and  $q_{r,t} = 0$  to  $q_{r,t} = q_{r,t}$  is represented by a hyperbolic equation:

$$q_{r,t} = \frac{q_{r,\max} t}{(1/k_r q_{r,\max}) + t}. \quad (3)$$

To simplify the experimental data fitting a novel constant can be defined,  $(1/k_r q_{r,\max}) = t_{1/2}$ . Physically this novel constant represents the time at which the half of the maximal removed quantity of uranyl was reached. In the current study  $t_{1/2}$  is called the “half-removal time” and it makes it possible to calculate the initial rate of uranyl-ion removal using the following expression:

$$v_0 = \frac{q_{r,\max}}{t_{1/2}} = k_r(q_{r,\max})^2. \quad (4)$$

The fitting of experimental kinetic curves ( $q_{r,t}$  vs  $t$ ) using Eq. (3) is shown in Fig. 3. The parameters  $t_{1/2}$  and  $q_{r,\max}$  were estimated by applying a nonlinear regression by least squares method performed with SigmaPlot software (see Table 1).

On the other hand, the initial rate of uranyl removal  $v_0$ , and the maximal removed quantity of uranyl  $q_{r,\max}$ , are a function of, for example, the initial concentration of uranyl, the temperature, the dose and nature of solid particles (of manganese oxide), and the pH of solution. The approach proposed in this study considers only the variation of the initial concentration of uranyl (see Table 1); i.e., in the experiments the temperature, the solid-particles/volume of solution ratio, and the pH of solution were fixed (see Section 2).

Concerning the variation of initial concentration of uranyl ion  $C_0$ , the initial rate of uranyl removal can be then represented as a function of initial concentration of uranyl ion ( $v_0 = f(C_0)$ ). This function can be fitted assuming a one-site saturation model, a two-sites saturation model, or a multisites saturation model. For this study, a one-site saturation model was

Table 1

Fitting kinetic parameters for removal of uranyl ion from aqueous solution onto synthetic manganese oxide

$C_0$ [ $\mu\text{mol/L}$ ]	$q_{r,\max}$ [ $\mu\text{mol/g}$ ]	$t_{1/2}$ [min]	$r$ (correlation factor)	$v_0$ [ $\mu\text{mol/g min}$ ]
0.28	$0.062 \pm 0.003$	$4.5 \pm 1.4$	0.9605	0.014
2.27	$0.399 \pm 0.007$	$2.4 \pm 0.3$	0.9947	0.169
5.50	$0.666 \pm 0.026$	$1.8 \pm 0.8$	0.9600	0.371
11.86	$0.767 \pm 0.024$	$1.3 \pm 0.4$	0.9842	0.606

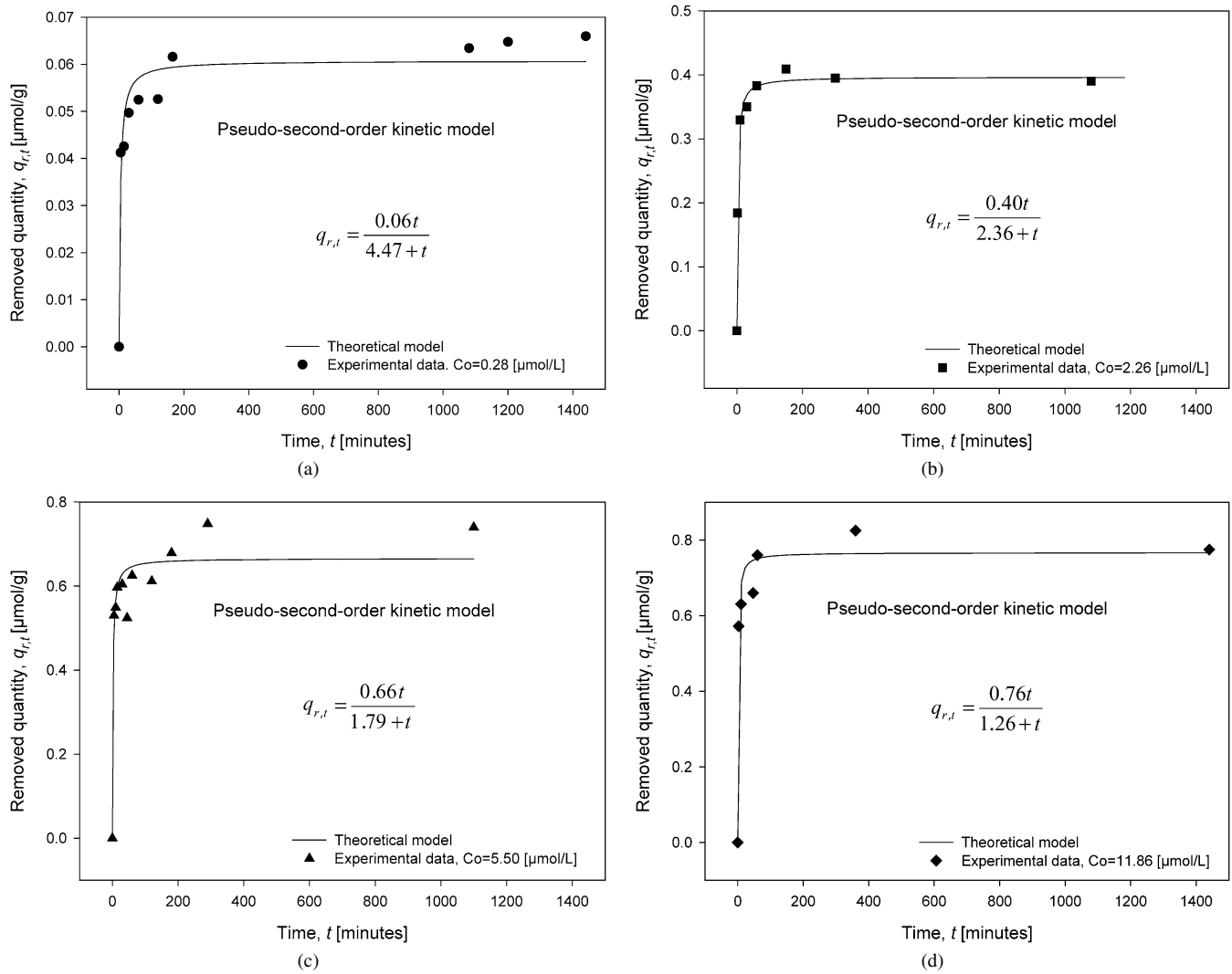


Fig. 3. Fitting of experimental data for removal of the uranyl ion from aqueous solution onto synthetic manganese oxide. (a)  $C_0 = 0.28 \mu\text{mol/L}$ , (b)  $C_0 = 2.27 \mu\text{mol/L}$ , (c)  $C_0 = 5.50 \mu\text{mol/L}$ , (d)  $C_0 = 11.86 \mu\text{mol/L}$ .

considered because this has a good correlation with experimental data; the differential form of the equation can be written

$$\frac{dv_0}{dC_0} = k_{v0}(v_{0,\max} - v_0)^2, \quad (5)$$

where  $k_{v0}$  is a complex kinetic constant of uranyl removal [ $\text{g min L}/\mu\text{mol}^2$ ],  $v_{0,\max}$  is the maximal rate of uranyl removal [ $\mu\text{mol/g min}$ ],  $v_0$  is the initial rate of uranyl removal [ $\mu\text{mol/g min}$ ], and  $C_0$  is the initial concentration of uranyl [ $\mu\text{mol/L}$ ].

The integrated form of Eq. (5) for the boundary conditions  $C_0 = 0$  to  $C_0 = C_0$  and  $v_0 = 0$  to  $v_0 = v_0$  can be written

$$v_0 = \frac{v_{0,\max} C_0}{(1/k_{v0} v_{0,\max}) + C_0}, \quad (6)$$

where  $k_{v0} v_{0,\max} = K$  can be interpreted as the initial uranyl-removal coefficient [ $\text{L}/\mu\text{mol}$ ]. Then Eq. (6) can be rearranged to obtain

$$v_0 = \frac{v_{0,\max} K C_0}{1 + K C_0}. \quad (7)$$

This model is equivalent to the Langmuir–Hinshelwood equation sometimes published in the literature; see for example [30,31].

The fitting of data  $v_0$  vs  $C_0$  using Eq. (7) allows the estimation of  $v_{0,\max}$  and  $K$ . For this case, a nonlinear regression by least-squares method was performed with SigmaPlot software (see Fig. 4). This figure shows that the one-site saturation model has a strong correlation with the estimated-experimental data of uranyl removal, yielding a value of  $1.45 \mu\text{mol/g min}$  for  $v_{0,\max}$  and a value of  $0.06 \text{ L}/\mu\text{mol}$  for  $K$ . This estimate is valid for the concentration range of uranyl ions taken into account in this study. Unpublished data showed that high concentrations of uranyl ions ( $>25 \mu\text{mol/L}$ ) in the system produce complex behavior in the solid–liquid interactions (e.g., kinetic sorption–desorption process, possibly the activation of other site types, etc.).

The maximal rate of uranyl removal,  $v_{0,\max}$ , estimated by Eq. (7) and now given in [ $\text{mol/g s}$ ] allows the calculation of a mass transfer coefficient  $D_{\text{transfer}}$  [ $\text{m}^2/\text{s}$ ] using the relation

$$D_{\text{transfer}} = v_{0,\max} N m \bar{a}, \quad (8)$$

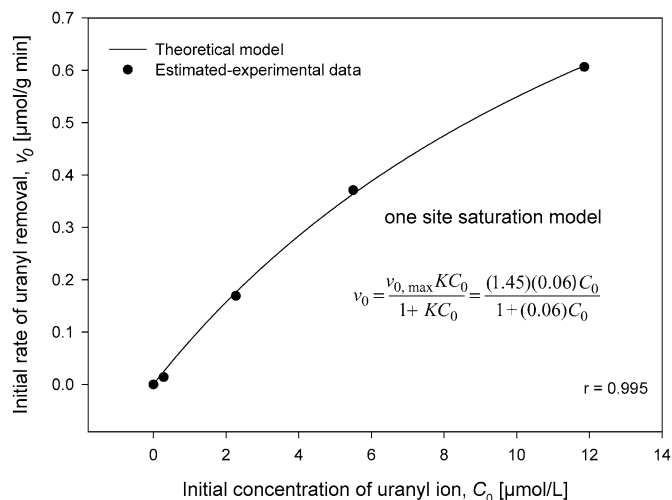


Fig. 4. Fitting of initial rate of uranyl removal as a function of initial concentration of uranyl ion.

where  $N$  is the Avogadro number ( $6.0221353 \times 10^{23}$  ions/mol),  $m$  is the mass of solid particles of manganese oxide dispersed in the reactor (1 g), and  $\bar{a}$  is the cross-sectional area of the uranyl ion [ $\text{m}^2$ ]. It was shown by speciation calculations that  $\text{UO}_2^{2+}$  is the dominant species in the experimental solutions. The cross-sectional area was thus assumed to be equal to the surface of the equatorial plane of the uranyl moiety. In aqueous media, uranyl ions usually display five or six atoms of oxygen in this plane, with a  $\text{U}-\text{O}_{\text{eq}}$  bond length ranging from 2.3 to 2.5 Å [32]. With a mean value of 2.4 Å and five equatorial  $\text{O}_{\text{eq}}$ , the cross-sectional area would be equal to  $1.36 \times 10^{-19} \text{ m}^2$ . A maximum value of this area can be calculated by assuming a surface equal to a disc with a radius of 2.4 Å ( $\bar{a}_{\text{max}} = 1.8 \times 10^{-19} \text{ m}^2$ ). As expected, the value calculated by Eq. (8) ( $2.64 \times 10^{-3} \text{ m}^2/\text{s}$ ) shows that the mass transfer in a dispersed reactor is very high compared with the mass transfer (effective diffusion coefficient) in a porous medium, for example, a ferromanganese crust medium ( $\cong 1 \times 10^{-10} \text{ m}^2/\text{s}$ ) [33].

The coefficient value calculated by Eq. (8) represents only the external mass transfer and evidently this calculation does not indicate if the removal process is governed by external mass transfer (boundary layer diffusion) or by intraparticle diffusion. To characterize the rate-controlling step involved in the uranyl removal process, the removal data could be analyzed with the Boyd equation,  $-\ln[1 - (q_{r,t}/q_{r,\text{max}})] = kt$ , where  $q_{r,t}$  represents the removed quantity of uranyl ion at any time  $t$  [ $\mu\text{mol/g}$ ],  $q_{r,\text{max}}$  represents the maximal removed quantity of uranyl ion or removed quantity of uranyl ion at equilibrium [ $\mu\text{mol/g}$ ], and  $k$  represents the constant rate of removal process [34]. The linearity of the  $kt$  vs  $t$  plot should provide useful information to distinguish between external-transport and intraparticle-transport-controlled rates of removal process. For example, a linear plot indicates that, for the studied solute concentration range, external mass transport mainly governs the rate-limiting process. It is necessary to remark that the Boyd equation can be derived by a pseudo-first-order kinetic model. Thus, the Boyd equation must be taken with care because the kinetic process, in the current study, was treated by a pseudo-second-order kinetic model.

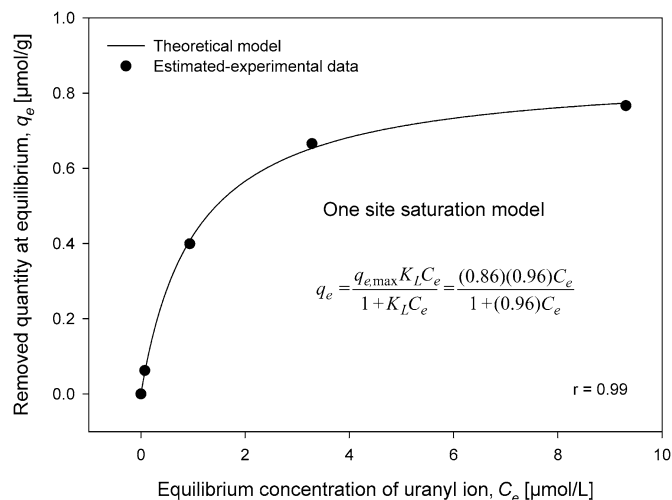


Fig. 5. Fitting of removed quantity at equilibrium as a function of equilibrium concentration of uranyl ion.

### 3.3. Removal of uranyl ions at equilibrium

Equation (5) (see above) describes the initial rate of the uranyl-removal process as a function of the initial concentration of uranyl ion ( $v_0 = f(C_0)$ ). Obviously, this equation can also be written in terms of the maximal removed quantity of uranyl ion at equilibrium ( $q_{r,\text{max}} = q_e$ ) and the equilibrium concentration of uranyl ion,  $C_e$  ( $q_e = f(C_e)$ ). Then, assuming, one-site saturation model, the differential form of the equation can be written as

$$\frac{dq_e}{dC_e} = k_{q_e}(q_{e,\text{max}} - q_e)^2, \quad (9)$$

where  $k_{q_e}$  is a complex constant of the removal process [ $\text{g L}/\mu\text{mol}^2$ ],  $q_{e,\text{max}}$  is the maximal removed quantity of uranyl ions at equilibrium [ $\mu\text{mol/g}$ ],  $q_e$  is the removed quantity of uranyl ions at equilibrium [ $\mu\text{mol/g}$ ], and  $C_e$  is the equilibrium concentration of solute [ $\mu\text{mol/L}$ ].

The integrated form of Eq. (9) for the boundary conditions  $C_e = 0$  to  $C_e = C_e$  and  $q_e = 0$  to  $q_e = q_e$ , can be written as

$$q_e = \frac{q_{e,\text{max}} C_e}{1/k_{q_e} q_{e,\text{max}} + C_e}, \quad (10)$$

where  $(k_{q_e})(q_{e,\text{max}}) = K_L$  can be interpreted as the equilibrium uranyl-removal coefficient [ $\text{L}/\mu\text{mol}$ ]. Equation (10) can be then rearranged to obtain the Langmuir equation:

$$q_e = \frac{q_{e,\text{max}} K_L C_e}{1 + K_L C_e}. \quad (11)$$

The fitting of  $q_e$  vs  $C_e$  using Eq. (11) allows the estimation of  $q_{e,\text{max}}$  and  $K_L$ . For this case, a nonlinear regression by least-squares method was performed with SigmaPlot software (see Fig. 5).

Consequently, the equilibrium uranyl-removal coefficient  $K_L$  ( $0.96 \text{ L}/\mu\text{mol}$ ) can be used to calculate a dimensionless constant separation factor or equilibrium parameter  $K_s$ , which is considered as a more reliable indicator of ion removal process (in fixed-bed or batch systems) [35]. This parameter is defined by the relationship

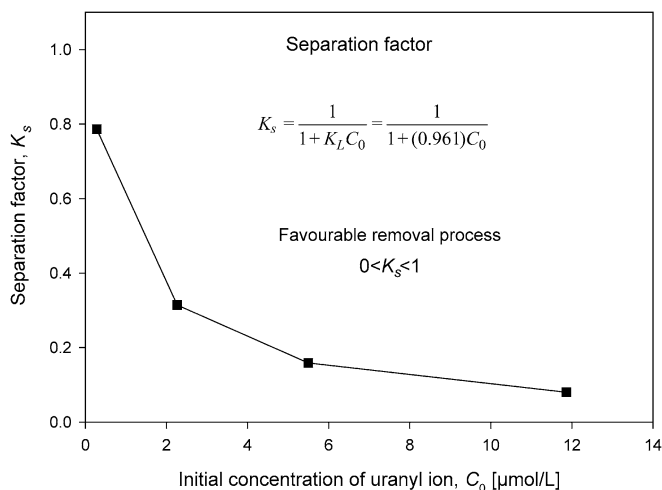


Fig. 6. Separation factor behavior as a function of initial concentration of uranyl ion.

$$K_s = \frac{1}{1 + K_L C_0}, \quad (12)$$

where  $K_s$  is a dimensionless separation factor,  $C_0$  is initial concentration of uranyl ions [ $\mu\text{mol/L}$ ], and  $K_L$  is the equilibrium uranyl-removal coefficient [ $\text{L}/\mu\text{mol}$ ]. For a favorable removal process,  $0 < K_s < 1$ , while  $K_s > 1$  represents an unfavorable removal process, and  $K_s = 1$  indicates a linear removal process. If  $K_s = 0$  the removal process is irreversible. For the concentration range considered in this study, the removal process of uranyl ions is favorable (see Fig. 6).

The maximal removed quantity of uranyl ions at equilibrium  $q_{e,\text{max}}$  estimated by Eq. (11), equal to  $0.86 \mu\text{mol/g}$ , can be assumed to correspond to the saturation of some high-affinity sites. Previous studies have established that sorption on birnessite consists of ion exchange at interlayer sites and pH-dependent sorption at specific sites usually corresponding to the vacancies on the  $\text{MnO}_6$  sheet [4–6,20,21]. Alkali and alkaline earth metal ions with large ionic radii are located in interlayer sites, whereas metal ions seem more likely to be connected to vacancy sites. The high rate of uranyl sorption on the birnessite observed in this study (significantly higher than the rate of Na desorption from interlayer sites measured during the equilibration period, for instance) and the strong geometrical constraint due to the size and shape of the uranyl moiety both assert against the diffusion of uranyl inside the interlayer of the mineral. Instead, sorption at the crystallite edge sites can be inferred. The saturation of uranyl high-affinity sites would then correspond to a density of edge sites equal to  $0.047 \text{ sites}/\text{nm}^2$ , taken into account the specific surface area of  $11 \text{ m}^2/\text{g}$  measured for the solid phase. This density might be compared to the density of vacant sites at the birnessite surface. If the  $\text{MnO}_2(110)$  plane is used as a model surface, a total density of  $10 \text{ Mn sites}/\text{nm}^2$  can be calculated. The chemical formula of low-pH birnessite determined by Drits et al. and Silvester et al. [17,18] implies that 17% of the layer of Mn octahedra are vacant. This amount yields a density of  $1.7 \text{ vacant sites}/\text{nm}^2$  at the surface of the birnessite crystallites. The maximum surface coverage of the uranyl ions represents thus about 3% of vacant sites in the Mn layer.

## 4. Conclusions

The experimental–theoretical approach presented in this study allowed the description and estimation of kinetic and thermodynamic parameters for the removal of uranyl ion ( $\text{UO}_2^{2+}$ ) from aqueous solutions onto synthetic manganese oxide by using kinetic studies with dispersed batch reactors; i.e., the removed quantity of uranyl ion was found as a function of time at different initial concentrations.

These basic parameters will allow the optimization of an ion-removal process for dispersed batch reactors at a laboratory scale, and then they will also facilitate the extrapolation of an ion-removal process for dispersed flux-continuous reactors at a pilot scale.

Finally, pseudo-second-order kinetics and one-site saturation models allowed a mechanistic analysis of the uranyl removal process in dispersed batch reactors.

## Acknowledgments

The authors are grateful to UMR 7517 ULP-CNRS-CGS, France, for providing a financial grant for this work. A. Manceau and M. Musso are thankful for the advice on the synthesis of birnessite. This is CGS-EOST Contribution CN 2006.201-UMR7517.

## References

- [1] J.R. Bargar, S.N. Towle Jr., G.E. Brown, G.A. Parks, *J. Colloid Interface Sci.* 185 (1997) 473.
- [2] W. Wang, J.T.C. Kwak, *Colloids Surf. A* 156 (1999) 95.
- [3] L. Huang, C. Maltesh, P. Sumasundaran, *J. Colloid Interface Sci.* 177 (1996) 222.
- [4] J. Post, *Proc. Natl. Acad. Sci. USA* 96 (1999) 3447.
- [5] E.A. Jenne, in: R.F. Gould, (Ed.), *Trace Inorganics in Water*, Am. Chem. Soc. Adv. Chem. Ser. 337 (1967).
- [6] A. Manceau, V.A. Drits, E. Silvester, C. Bartoldi, B. Lanson, *Am. Mineral.* 82 (1997) 1150.
- [7] A. Manceau, B. Lanson, V.A. Drits, *Geochim. Cosmochim. Acta* 66 (2002) 2639.
- [8] B. Lanson, V.A. Drits, A.C. Gaillot, E. Silvester, A. Plançon, A. Manceau, *Am. Mineral.* 87 (2002) 1631.
- [9] T. Allard, P. Ildefonse, C. Beaucaire, G. Calas, *Chem. Geol.* 158 (1999) 81.
- [10] D.M. Bonotto, *J. South Am. Sci.* 11 (1998) 389.
- [11] R.F. Anderson, M.P. Bacon, P.G. Brewer, *Earth Planet. Sci. Lett.* 66 (1983) 73.
- [12] A. Herczeg, J. Simpson, R. Anderson, R. Trier, G. Mathieu, B. Deck, *Chem. Geol.* 72 (1988) 181.
- [13] M.C. Duff, D.B. Hunter, *Environ. Sci. Technol.* 33 (1999) 2163.
- [14] V.M. Burns, R.G. Burns, *Earth Planet. Sci. Lett.* 39 (1978) 341.
- [15] F.V. Chukhrov, B.A. Sakharov, A. Gorshkov, V.A. Drits, Y.P. Dikov, *Int. Geol. Rev.* 27 (1985) 1082.
- [16] R.M. Cornell, R. Giovanoli, *Clays Clay Miner.* 36 (1988) 249.
- [17] V.A. Drits, E. Silvester, A. Gorshkov, A. Manceau, *Am. Mineral.* 82 (1997) 946.
- [18] E. Silvester, A. Manceau, V.A. Drits, *Am. Mineral.* 82 (1997) 962.
- [19] B. Lanson, V.A. Drits, E. Silvester, A. Manceau, *Am. Mineral.* 85 (2000) 826.
- [20] A. Manceau, A. Gorshkov, V.A. Drits, *Am. Mineral.* 77 (1992) 1133.
- [21] A. Manceau, A. Gorshkov, V.A. Drits, *Am. Mineral.* 77 (1992) 1144.
- [22] A. Manceau, N. Tamura, R. Celestre, A. McDowell, N. Geoffroy, G. Spósito, H. Padmore, *Environ. Sci. Technol.* 37 (2003) 75.

- [23] A. Manceau, C. Tommaseo, S. Rihs, N. Geoffroy, D. Chateigner, M. Schlegel, D. Tisserand, M.A. Marcus, N. Tamura, Z.S. Chen, *Geochim. Cosmochim. Acta* 69 (2005) 4007.
- [24] R. Giovanoli, E. Stähli, W. Feitknecht, *Helv. Chim. Acta* 53 (1970) 454.
- [25] L.S. Balistrieri, J.W. Murray, *Geochim. Cosmochim. Acta* 46 (1982) 1041.
- [26] J.D. Allison, D.S. Brown, N.K. Novo-Gradac, MINTEQA2: A geochemical assessment model for environmental systems, U.S. EPA, Athens, Georgia, 1991.
- [27] I. Grenthe, J. Fuger, R. Konings, R.J. Lemire, A.B. Muller, C. Nguyen-Trung, J. Wanner, *Chemical Thermodynamics of Uranium*, North-Holland, Amsterdam, 1992.
- [28] R.J. Silva, *Mater. Res. Soc. Symp. Proc.* 257 (1992) 323.
- [29] M.E. Torrero, I. Casas, J. De Pablo, M. Sandino, B.A. Grambow, *Radiochim. Acta* 66–67 (1994) 29.
- [30] O. Zahraa, H.Y. Chen, M. Bouchy, J. Adv. Oxid. Technol. 4 (1999) 167.
- [31] A.H.C. Chan, J.F. Porter, J.P. Barford, C.K. Chan, *Water Sci. Technol.* 44 (2001) 187.
- [32] P.C. Burns, R.C. Ewing, F.C. Hawthorne, *Can. Mineral.* 35 (1997) 1551.
- [33] G.M. Henderson, K.W. Burton, *Earth Planet. Sci. Lett.* 170 (1999) 169.
- [34] G.E. Boyd, A.W. Adamson, L.S. Meyers, *J. Am. Chem. Soc.* 69 (1947) 2836.
- [35] Y.S. Ho, C.T. Huang, H.W. Huang, *Process Biochem.* 37 (2002) 1421.